Advances in Colloid and Interface Science
100–102 (2003) 613–639

ADVANCES IN COLLOID AND INTERFACE SCIENCE

www.elsevier.com/locate/cis

Sedimentation–diffusion profiles and layered sedimentation of charged colloids at low ionic strength

Albert P. Philipse*, Gijsberta H. Koenderink

Van't Hoff Laboratory for Physical and Colloid Chemistry, Debye Institute, Utrecht University, Padualaan 8, 3584 CH Utrecht, The Netherlands

Received 12 August 2002; accepted 27 August 2002

Abstract

We report the formation of strongly inflated sedimentation–diffusion concentration profiles for charged monodisperse colloidal spheres in absolute ethanol. Various additional experiments, such as light scattering, confirm that the very dilute supernatants, left behind by the majority of settling colloids, contain spheres that repel each other at distances of micrometers. We attribute these unusual profiles to a significant counter-ion contribution to the osmotic pressure and to the Debye screening length. An approximate osmotic equation-of-state at the level of the second virial coefficient for dispersions at very low ionic strength indeed implies an algebraic long-distance decay of sedimentation–diffusion profiles, together with significant lowering of the effective colloid mass by an entropic lift due to counter-ions. We have also observed that sedimenting dispersions sometimes demix into two layers, which are both disordered fluids. Since the colloids are clearly repulsive on the DLVO pair level, this layering possibly manifests a phase transition driven by many-body attractions.

Keywords: Charged colloids; Sedimentation; Sedimentation–diffusion equilibrium; Silica spheres; Phase transition

*Corresponding author. Tel.: +31-30-253-2391; fax: +31-30-253-3870.
E-mail address: fccoffice@chem.uu.nl (A.P. Philipse).

0001-8686/03/$ - see front matter
PII: S0001-8686(02)00078-7

1. Introduction

The DLVO theory [1] quantifies the double-layer repulsion between two charged colloidal spheres in a large electrolyte reservoir of 'external salt' with fixed ionic strength, such that the Debye screening length is constant and unaffected by the counter-ions produced by the colloids. In other words, the pair potential for the colloids is assumed to be independent of the colloid number density. In dispersions of very low ionic strength this assumption will not hold, because at sufficiently high colloid concentration the counter-ions contribute significantly to the total electrolyte concentration. As a result the colloids interact via density-dependent repulsion, which is of long range due to the low salt content [2]. In de-ionised or organic solvents [3] the Debye length may even be in the micrometer range, in which case concentration or many-body effects may already be significant at low colloid densities. One widely debated consequence of such effects is the possibility of a liquid–gas phase transition in a system of colloids with purely repulsive DLVO pair-potentials [4–11]. The cohesive energy that stabilises the liquid phase, it is argued [9], is provided by the Coulomb attraction between colloids and their counter-ions, which is reminiscent of the liquid–vapour coexistence predicted for molecular electrolytes [12,13]. Whether such phase behaviour related to counter-ions really occurs in colloidal dispersions is—at least from the experimental point of view—still questionable. A crucial observation would be a macroscopic meniscus separating two disordered fluids, with rigorous exclusion of artefacts, and clear proof that particles are repulsive at the pair level. Findings on charged colloids reported in this contribution support—and indeed perhaps even demonstrate—the possibility of a Van der Waals-like instability in the osmotic equation of state. They do, in any case, point to an important contribution of counter-ions to the osmotic pressure, which we traced by unusual concentration profiles in sedimenting dispersions.

The sedimentation–diffusion (SD) equilibrium is a balance between osmotic pressure gradients and external (gravitational or centrifugal) forces on colloidal particles. The equilibrium profile is of fundamental interest, because it is equivalent to the osmotic equation of state. The profile is quite sensitive to interactions between the colloids and, in principle, the profile can be integrated to obtain an accurate osmotic equation of state over a wide density range [14–16]. For the case of ideal, non-interacting colloids the osmotic pressure is given by Van't Hoff's law, and the corresponding equilibrium SD density profile is a single exponential decay. For charged colloids interacting through a DLVO potential, the deviation from a single exponential will be modest for a low concentration of colloids in an electrolyte solution of sufficient ionic strength such that the Debye screening length is small, though large enough to avoid flocculation. We also expect that the thickness of the ideal exponential decay is still a relevant measure for the spatial extension of the non-ideal profile. For strongly interacting, charged spheres at low ionic strength, the functional form of the SD profile may change considerably. From theory and simulations by Biben et al. [15,16] we expect in this case an SD profile with an almost linear decay at nearly all altitudes.

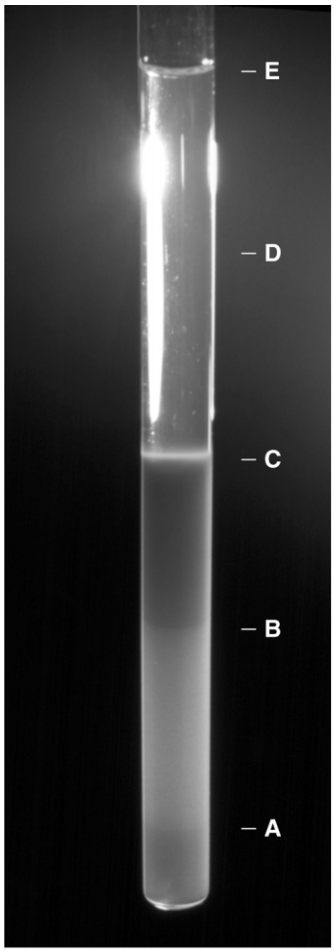

Fig. 1. A dispersion of silica spheres (type C, see Table 1) with initial volume fraction of approximately 0.01 in absolute ethanol, stored in a thermostatted room sedimenting in a tube with diameter of 1 cm. Several layers can be distinguished. A is the top of the sediment at the bottom of the tube. B is the interface between two regions of different density in the sedimenting dispersion. C is the steep concentration decrease upon entering the supernatant phase D. The bluish Tyndall scattering in D manifests the presence of a very dilute dispersion up to the solvent–air interface E.

In our laboratory, however, we observed many instances of sedimenting charged spheres that seem at odds with these expectations (Figs. 1 and 2). The observations relate to stock suspensions of charged silica spheres in ethanol, which have settled under gravity for periods of 1 month to more than 10 years. The interface separating the sedimenting (or sedimented) suspension and supernatant liquid is usually fairly sharp. The general feature of these supernatants is the presence of a low but significant concentration of colloidal spheres, as manifested by a bluish (Tyndall)

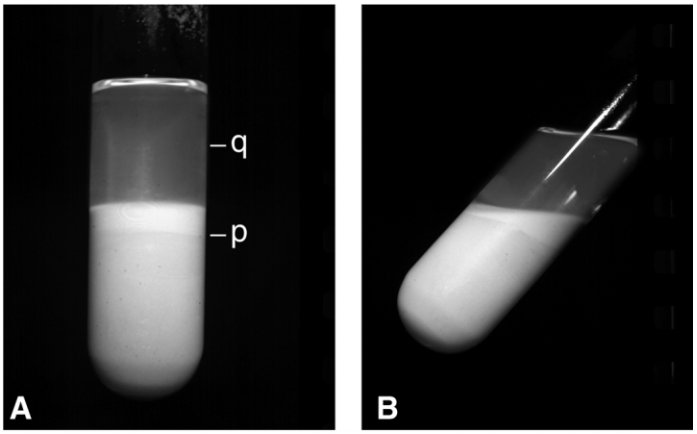

Fig. 2. Silica spheres in ethanol used in [36]. The sample was left undisturbed in a closed cupboard for 13 years. Interface p manifests a phase equilibrium (see text). Supernatant q is a dilute dispersion.

turbidity or visible laser-light scattering. The spatial extension of these supernatants is orders of magnitude larger than expected from any reasonable estimate of the barometric height distribution for non-interacting uncharged spheres. Moreover, the sediment–supernatant interface corresponds to a steep concentration gradient, which is difficult to understand on the basis of the work of Biben et al. [15,16]. Another intriguing feature we sometimes observed is the presence of several (non-crystalline) layers in a sedimenting suspension. Fig. 1 shows a beautiful example for a dispersion of silica spheres in ethanol stored in a thermostatted room. Such layering, if it is a truly thermodynamic phenomenon, is quite puzzling; how can it be present at all for monodisperse colloids interacting through a repulsive DLVO potential? The work of van Roij and co-workers [6–9] suggested to us the idea that the layering as illustrated in Fig. 1 perhaps signals a many-body phase transition. This possibility, together with the observation of the extended SD profiles mentioned above, motivated us to re-examine the behaviour of charged spheres in ethanol.

Our strategy was to verify in the first place which of these observations would persist for sedimentation under well-defined conditions, because observations for stock suspensions stored without any precautions in a laboratory cupboard may be very misleading. It is well known, for example, that mechanical vibrations, thermal convections and light [17,18] easily disturb sedimenting suspensions, so it is possible that unusual concentration profiles are actually non-equilibrium artefacts caused by convections. We note here the stratification due to temperature gradients [19,20], the stir in suspensions by light-absorbing colloids [18] and the layering that may inherently occur in polydisperse samples [15]. Furthermore, contaminants may be introduced by mixed-bed resins for de-ionisation. Therefore, we only used absolute ethanol without any resin. Since the background electrolyte concentration in ethanol may be as low as 10^{-9} M, the effect of counter-ions on SD profiles needs to be

addressed. To the best of our knowledge, however, there are no calculations for concentration profiles of colloids with a density-dependent potential. Therefore, we employ in Section 2 a simple excluded-volume model to show that the counter-ion effect may be substantial, leading to profiles with a slowly decaying algebraic tail. In the experimental section we discuss the formation and features of concentration profiles of silica spheres settling under gravity in pure ethanol without added salt. These are first results from an ongoing study, published for the occasion of this special issue for Prof. Overbeek, at a time when some features of SD profiles are becoming clear, whereas our understanding of layering as in Figs. 1 and 2 is still limited.

2. Theoretical

2.1. Non-interacting spheres

In de-ionised water and polar organic solvents such as ethanol, the screening of double-layer repulsions is weak and charged colloids may interact over micrometer distances. Thus, at low ionic strength very low colloid concentrations are required to achieve the limit of non-interacting colloids. Sometimes 'infinite dilution' is experimentally hardly accessible; witness the sedimentation rate of charged silica spheres in de-ionised ethanol, which is known to be concentration-dependent down to very low concentrations [21]. Nevertheless, the case of non-interacting charged spheres is of interest as an illustrative example of the effect of counter-ions on the SD equilibrium profile. In such a profile an external force K acting on each colloid is balanced by the equilibrium gradient in osmotic pressure, which under isothermal conditions only depends on the local number density ρ at altitude x:

$$\frac{d\Pi}{dx} = -\rho(x)K \tag{1}$$

If ρ obeys Van't Hoff's law for the osmotic pressure, $\Pi = \rho kT$, the SD equilibrium profile from Eq. (1) is the well-known single exponential decay:

$$\ln\frac{\rho(x)}{\rho_0} = -\frac{x}{l_g} \tag{2}$$

where ρ_0 is the density at the bottom $(x=0)$ of the sedimentation vessel. The distance x is scaled on the gravitational length:

$$l_g = \frac{kT}{K} = \frac{kT}{\Delta mg} \tag{3}$$

for colloids with weight Δmg, where Δm is the particle mass corrected for buoyancy. This gravitational length is a measure of the thickness of the exponential concentration profile. It is, in fact, the average distance from the colloids to the bottom of the vessel:

$$\langle x\rangle = \frac{\int_0^\infty \exp\left[-x/l_g\right] x\,\mathrm{d}x}{\int_0^\infty \exp\left[-x/l_g\right]\mathrm{d}x} = l_g \tag{4}$$

Suppose each colloid carries a constant number of z charges. Even if the colloids do not interact with each other, the counter-ions may already influence the SD profile considerably. This influence can be understood as a straightforward consequence of the classical Donnan equilibrium, in which colloids are separated from a large electrolyte reservoir by a membrane that only allows water and salt to permeate. At both sides of the membrane the chemical potentials of solvent and ions are equal, and the dispersion and reservoir are both electrically neutral bulk solutions. The osmotic (excess) pressure of the colloidal dispersion resulting from the equilibrium and electroneutrality conditions, taking all solutes as ideal, is (see e.g. [22]):

$$\frac{\Pi}{kT} = \rho + 2\rho_{el}\left[\sqrt{1+s^2}-1\right] \tag{5}$$

The Donnan pressure contains the linear ρ term for ideal, uncharged colloids, plus a term that depends on

$$s = \frac{z\rho}{2\rho_{el}} \tag{6}$$

which is a measure of the counter-ion concentration $z\rho$ relative to the constant ion concentration $2\rho_{el}$ in the large reservoir. Suppose that a SD profile is present in a Donnan set-up (Fig. 3) such that Donnan equilibrium occurs at any height x. Substitution of Eq. (5) into Eq. (1) shows that this SD profile following from the Donnan pressure is given by:

$$(1+z)\ln\frac{\rho(x)}{\rho_0} + z\ln\frac{1+\sqrt{1+s^{-2}(x)}}{1+\sqrt{1+s_0^{-2}}} = -\frac{x}{l_g} \tag{7}$$

where $s(x)$ is the value of s for a colloid number density $\rho(x)$. The second term on the left-hand side is set by the external salt concentration. At high salt concentration ($s \ll 1$) the dependence of this second term on s vanishes, and the SD profile, as expected, reduces to the single exponential of non-interacting uncharged particles in Eq. (2). At very low external ionic strength ($s \gg 1$) an exponential is also found, but now with a gravitational length increased by a factor of $(1+z)$:

$$\ln\frac{\rho(x)}{\rho_0} = -\frac{x}{l_g(1+z)} \tag{8}$$

The physical meaning of this interesting limiting case is as follows. In the Donnan equilibrium all components are ideal (i.e. obey Van't Hoff's law), so the effect of the attraction between colloids and their counter-ions on the osmotic pressure is also

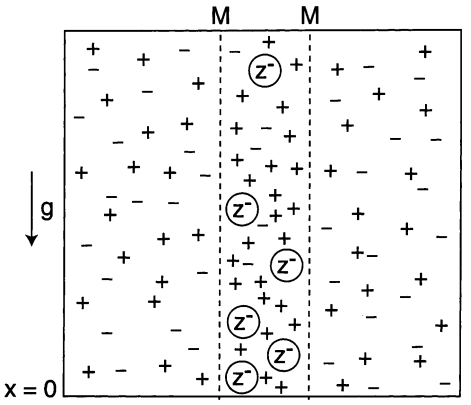

Fig. 3. Schematic of an inhomogeneous Donnan equilibrium in a gravitational field g. The colloids are confined between membranes M permeable only to ions and solvent. At every height x there is osmotic equilibrium between the colloids and a large electrolyte reservoir, which fixes the background electrolyte concentration ρ_{el}. Note that this sketch actually represents sedimentation–diffusion equilibrium in a dialysis tube with dispersion, vertically suspended in an electrolyte vessel.

neglected. The colloid density is nevertheless coupled to the counter-ion density by the condition of macroscopic electroneutrality. The $1z$ term is therefore purely entropic: small counter-ions gain entropy by leaving the thin SD profile of the large colloids to enter the nearly salt-free solvent. Thus, an electrical potential difference is produced which 'lifts up' the colloids to avoid macroscopic violation of electroneutrality. Stated differently: the counter-ions reduce the effective mass and increase the diffusion coefficient of the colloids by a factor of $1+z$. This substantial effect (z may be of the order of 10^3) was also noted by Mysels in his instructive textbook [22].

2.2. Interacting spheres

Consider interacting colloidal spheres with an equation of state given by the virial series for the osmotic pressure:

$$\frac{\Pi}{kT} = \rho + \sum_{n=2} B_n \rho^n \tag{9}$$

where B_n is the nth virial coefficient. Substitution in the isothermal force balance [Eq. (1)] leads to the following implicit solution for $\rho(x)$:

$$\ln\frac{\rho(x)}{\rho_0} + \sum_{n=2} \frac{n}{n-1} B_n\left[\rho^{n-1}(x) - \rho_0^{n-1}\right] = -\frac{x}{l_g} \tag{10}$$

At the top of the SD profile the concentration is beyond some point low enough such that the decay again becomes exponential. The first-order correction on the

level of the second virial coefficient is:

$$\ln\frac{\rho(x)}{\rho_0}+2B_2\left[\rho(x)-\rho_0\right]=-\frac{x}{l_g} \tag{11}$$

This result, derived earlier by Biben et al. [15], illustrates the modest effect of repulsion in dilute dispersions of uncharged hard spheres on the spatial extension of the SD profile. (For the full SD profile at higher hard-sphere densities see [15,23,24].) In Eq. (10) we have neglected any counter-ions and any density dependence of the virial coefficients. This dependence may change the SD profile quite drastically, as can be observed from the effect of counter-ions on B_2. We estimate this effect in the following manner. The Debye length κ^{-1} of a solution containing ions with number density ρ_i and valency v_i follows from:

$$\kappa^2=4\pi r_b\sum\rho_i v_i^2 \tag{12}$$

where

$$r_b=\frac{e^2}{4\pi\varepsilon\varepsilon_0 kT} \tag{13}$$

is the Bjerrum length, i.e. the distance between two elementary charges when their Coulomb interaction energy equals the thermal energy kT in a solvent with dielectric constant $\varepsilon\varepsilon_0$. The background electrolyte contains a number density ρ_{el} of univalent electrolyte. The colloids produce a number density ρz of (mono-valent) counter-ions, and since the Debye length depends on all ion concentrations in the solution (with the exception of the charged colloids) Eq. (12) becomes [2]:

$$\kappa^2=\kappa_0^2+4\pi r_b\rho z\ ;\quad \kappa_0^2=8\pi r_b\rho_{el} \tag{14}$$

where κ_0^{-1} is the Debye length at zero colloid concentration. We now assign to the colloids an effective interaction diameter given by:

$$d_i=\sigma+\alpha\kappa^{-1}\ ;\qquad \alpha\geq 0 \tag{15}$$

in which σ is the hard-core diameter of the colloids. The excluded volume per sphere, i.e. the second virial coefficient B_2, equals that of a hard sphere with diameter d_i:

$$B_2=\frac{2}{3}\pi(\sigma+\alpha\kappa^{-1})^3=B_2^{HB}\left(1+\frac{\alpha}{\kappa\sigma}\right)^3 \tag{16}$$

where the superscript HB denotes a hard sphere with diameter σ. The choice of the effective diameter in Eq. (15) is justified by the fact that the second virial coefficient in the form of Eq. (16) is a reasonable estimate of the (numerical) exact B_2 for a DLVO repulsion. This point is further discussed in Appendix A. Note the peculiar property of the excluded volume in Eq. (16); it shrinks when the colloid density increases because the counter-ions injected into the solution reduce κ^{-1}. We now add a second virial term to the Donnan pressure in Eq. (5):

$$\frac{\Pi}{kT} = \rho + 2\rho_{el}\left[\sqrt{1+s^2}-1\right] + B_2\rho^2 \tag{17}$$

Inserting Eqs. (14), (16) and (17) yields:

$$\frac{\Pi}{kT} = \rho + 2\rho_{el}\left[\sqrt{1+s^2}-1\right] + B_2^{HB}\rho^2\left[1+\frac{\alpha}{\sigma\sqrt{\kappa_0^2+4\pi r_b z\rho}}\right]^3 \tag{18}$$

At very low ionic strength, when $s \gg 1$ and $\kappa\sigma \ll 1$, the pressure is approximately:

$$\frac{\Pi V_p}{kT} \approx (1+z)\phi + 4\alpha^3\left[24\frac{r_b}{\sigma}z\right]^{-3/2}\sqrt{\phi}, \quad \varphi \ll 1 \tag{19}$$

for colloids with hard-core volume V_p, volume fraction $\phi = \rho V_p$ and $B_2^{HB} = 4V_p$. The square-root term, caused by the density dependence of the effective diameter, may seem uncommon. Note, however, the occurrence of fractional density terms for transport properties at low ionic strength [21,25] and, of course, the square-root term in the Debye length itself. Substitution of Eq. (19) into the force balance Eq. (1) leads to the SD profile:

$$(1+z)\ln\frac{\phi(x)}{\phi_0} + 4\alpha^3\left[24\frac{r_b}{\sigma}z\right]^{-3/2}\left(\frac{1}{\sqrt{\phi_0}} - \frac{1}{\sqrt{\phi(x)}}\right) = -\frac{x}{l_g} \tag{20}$$

which forms quite a contrast to the first-order correction for non-ideality for hard spheres in Eq. (11). The already substantial effect of counter-ions on the ideal logarithmic term is now supplemented by a term that inflates the profile at low density. The unusual feature of this profile is that it does not become ideal at high altitude. Its asymptotic decay is:

$$\phi(x) \sim 16\alpha^6\left[24\frac{r_b}{\sigma}z\right]^{-3}\left(\frac{x}{l_g}\right)^{-2}, \qquad \phi(x) \ll \phi_0 \ll 1 \tag{21}$$

This algebraic long-distance tail has its origin in the inflation of electrical double layers of colloids, which diffuse to higher altitudes in the salt-free solvent (Fig. 4). The volume fraction, of course, cannot be taken arbitrarily low without invalidating at some point the assumption that the density of solvent ions is much lower than that of counter-ions. On the other hand, near the bottom of the profile, the increasing colloid density at some point induces higher-order terms in the osmotic pressure. Therefore, Eq. (20) only provides a qualitative estimate for the spatial extension of the top of an SD-profile.

3. Experimental: materials and methods

3.1. Colloidal suspensions

The colloids in this study (see Table 1) are negatively charged silica spheres with a narrow size distribution, dispersed in absolute ethanol (in all cases fresh Baker

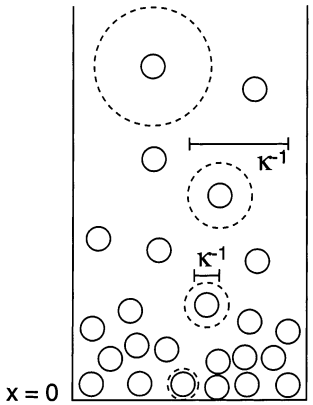

Fig. 4. Sketch of the origin of the algebraic long-distance tail of the SD profile at very low ionic strength: the diffuse double layer surrounding the colloids inflates at higher altitudes x.

p.a.). The spheres were initially prepared in an aqueous ethanol–ammonia mixture and subsequently silanised with 3-methacryloxypropyltrimethoxysilane (TPM) and finally transferred to pure ethanol by repeated sedimentation–redispersion procedures [26]. Four types of silica dispersions (see Table 1) were used in the sedimentation experiments to check any system dependence of our findings. A-Silica spheres contain the phosphorescent dye eosine isothiocyanate [27]. The other silica species (Table 1) are TPM-coated silica spheres without any dye.

3.2. Characterisation of particles and suspensions

Dynamic light scattering (DLS) was performed with an argon laser ($\lambda = 514.5$ nm) on samples from stock dispersions filtered through 0.2-μm FGLP Millipore membranes to make them dust-free. Static light scattering (SLS) was performed

Table 1
Properties of silica spheres

Code	Labcode	Sphere radius R (nm)	σ^b (%)	l_g^c (mm)
A	ESIMS [27]	90[a]	8	0.17
B	SIMS [27]	90[a]	8	0.17
C	SA6(2)TPM [26]	89[a]	8	0.16
D	NST 1	63[d]	9	0.50

[a] From static and dynamic light scattering. For C-spheres the value is the same as in [26].
[b] Polydispersity from electron micrographs.
[c] Estimate of gravitational length from Eq. (3) for non-interacting spheres of radius R in ethanol, using a particle mass density $\delta = 1.6$ g cm^{-3}.
[d] From AFM imaging.

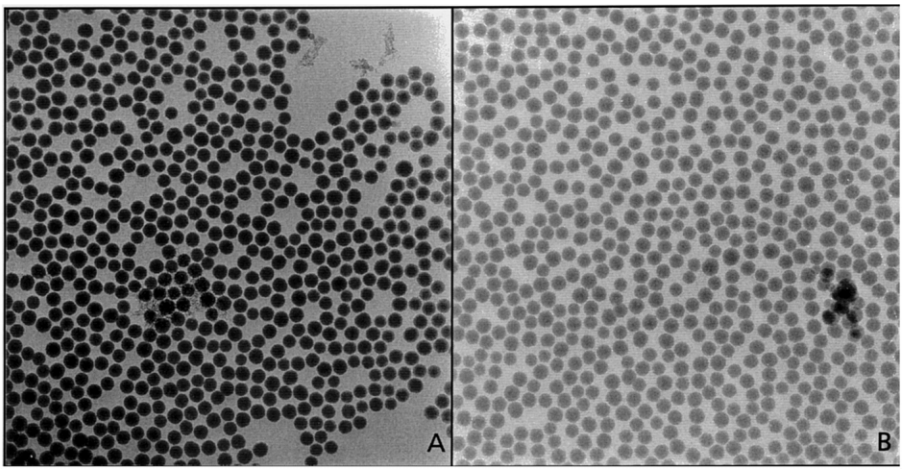

Fig. 5. Representative cryo-TEM micrographs of silica C-spheres in an ethanol glass film.

with a Fica-50 photometer ($\lambda = 564$ nm). Cryogenic transmission electron microscopy (cryo-TEM) was applied to dispersions of C-spheres in ethanol (Fig. 5). The technique images a film of dispersion after it has been glassified by shooting it into liquid ethane. The glassification of solvent is so rapid that the TEM image shows the distribution of colloids as present in the initial liquid film. Cryo-TEM is further explained in [28–32]. We note that imaging films from very dilute dispersions or supernatant is difficult because glassy solvent films with few particles are susceptible to mechanical or radiative damage. Atomic force microscopic (AFM) images of silica particles on poly-lysine-coated mica surfaces were made as described elsewhere [33].

3.3. Sedimentation experiments

Our silica particles (Table 1) are large enough to settle under gravity on a time scale of weeks. All sedimentation experiments were performed in vertical glass tubes stored undisturbed on a heavy marble table in a thermostatted ($T = 22.1 \pm 0.1$ °C) dark room in which samples were only illuminated for visual inspection, or for measurements of the position of interfaces between suspensions and their supernatants. These position measurements were done with a Zeiss Ni-40 levelling instrument coupled to a linear scale system (Mitutoyo AI-11-N), which allows height measurements with an uncertainty of 0.01 mm.

From stock vessels with known silica concentration, 5-ml volumes were pipetted into sample tubes (Fig. 6a), which were carefully screw-capped, sealed with Parafilm (American National Can PM-992), and placed precisely vertically in an airtight Perspex box under a nitrogen atmosphere. This box was intended to rule out any contamination of dispersions with carbon dioxide or water, which would change the

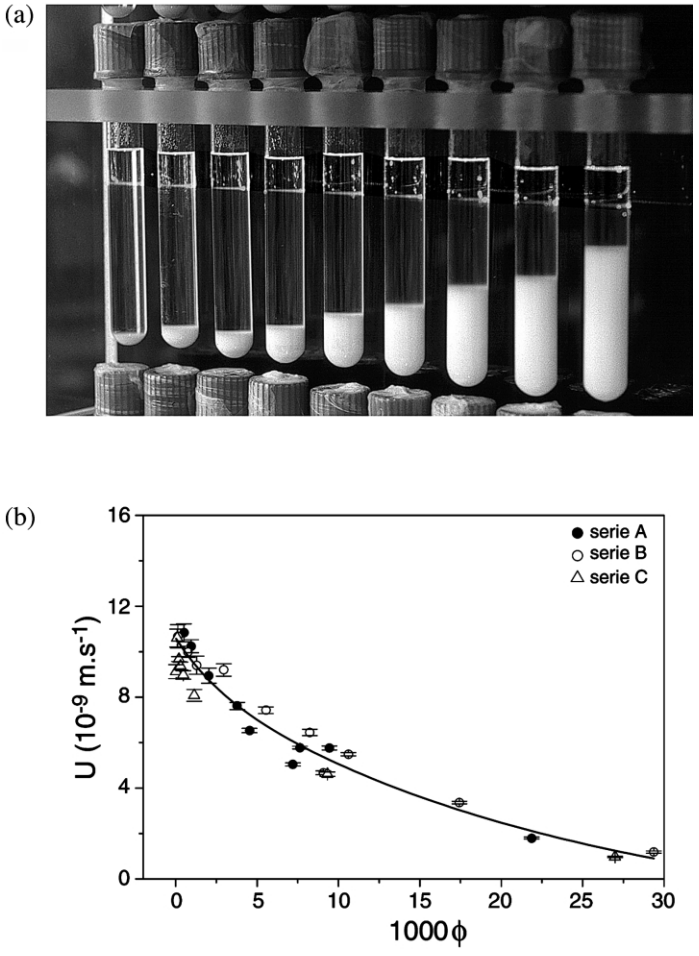

Fig. 6. (a) Sedimentation of C-spheres in absolute ethanol. Initial volume fractions range from 10^{-5} to 0.03. Situation after 12 weeks: the concentrated samples still sediment; the supernatants clearly contain colloids as evidenced by the red laser beam, which is observed here at a scattering angle of approximately 90°. (b) Sedimentation velocities $U(\phi)$ for A, B and C spheres vs. colloid volume fractions ϕ obtained from measuring the descendence of suspension–supernatant interfaces as in (a).

ionic strength. It was later found that the sealed tubes were sufficient for this purpose, because the electrical conductivity of ethanol in a sealed tube did not change over a period of several months.

For the glass tubes shown in Fig. 6 the supernatant volume was too small for concentration determination. Therefore, we repeated experiments with larger, gas-tight 500-ml glass bottles (Fig. 7), which were completely immersed in demi-water in a large aquarium (volume 120 l) in a dark thermostatted room to improve further the thermal isolation. The bottles were left undisturbed for periods ranging from 3

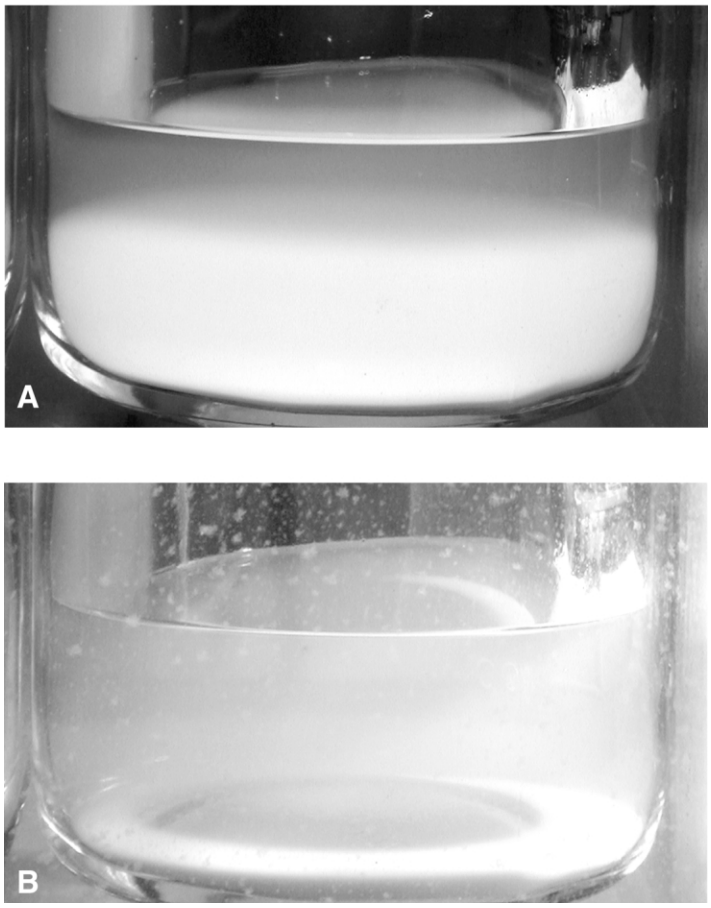

Fig. 7. Typical example of sedimentation in 0.5-l glass vessels immersed in thermostatted water. Settling C-silica spheres in picture (A) leave behind a turbid supernatant. Picture (B) was taken 4 months later: the majority of the monodisperse silica spheres have been deposited on the bottom. The supernatant liquid contains a fairly homogeneous dilute dispersion. [The spots on the outside of the bottle in (B) are due to algae and some rust from a stand keeping the bottle suspended.]

to 16 months. For comparison, some bottles were also stored in a closed thermostat in the thermostatted room. A concentration series of D-silica dispersions (Table 2) was stored in the aquarium for 6 months, after which 50-ml samples were pipetted from the supernatants without disturbing the sediment–supernatant interface. For bottles with a sufficient sediment volume, a sample of sediment was also pipetted. Particle weight concentrations were determined in duplicate from drying known volumes in aluminium foil cups to constant weight. Some D-silica dispersions were also sedimented in a table centrifuge for 20 h at 2000 rev. min^{-1} in glass vessels (Fig. 10), which were subsequently stored in thermostatted water. The aim was to

Table 2
Particle concentrations for sedimentation bottles immersed in water

Sample code	Concentration c (g l^{-1})		
	Initial	In 50 ml of supernatant	Sediment
C10	7.30	1.05	96.60
C15	4.87	0.25	94.60
C25	2.92	0.19	37.90
C40	1.83	0.37	70.70
C50	1.46	0.21	–
C100	0.73	0.64	–
C200	0.40	0.36	–

Samples were D-silica spheres in ethanol.

verify whether sediments would slowly expand over time, as expected for repulsive spheres [34], and whether particles would 'evaporate' to form a dilute supernatant.

4. Results and discussion

4.1. Choice of dispersions

First we motivate here the use of a dispersion of silica spheres silanised with TPM ('TPM–silica spheres') in ethanol as a colloidal model fluid characterised by dominant long-range repulsive pair interactions. The spheres do not flocculate in ethanol, even over extensive time intervals. The long-term stability of TPM–silica dispersions in ethanol is well documented [21,26,34–36] and is further confirmed by the fact that light-scattering radii of C-spheres did not change significantly over a period of 15 years (see Table 1). Dilute suspensions of TPM-coated silica spheres in ethanol have been widely studied and all available results from static and dynamic light scattering [26,36] and sedimentation [21,34,35] clearly confirm that the pair interaction is an electrical double-layer (DLVO) repulsion. It should also be noted that no unreacted silane-coupling agents (or TPM oligomers) are present, which might induce a depletion attraction between the spheres. The TPM coating is covalently linked to the silica surface and all unreacted TPM has been removed by repeated sedimentation–redispersion cycles [26]. The TPM coating is a multi-layer with a hydrodynamic thickness of approximately 2 nm. Since ethanol is a very good solvent for TPM [26], the layers repel each other and screen the van der Waals attraction between contacting spheres. In short, the only relevant interaction for the SD profile is that between electrical double layers. The double layer thickness may be substantial in pure ethanol, as can be observed as follows. Ethanol produces ions via:

$$2C_2H_5OH \rightarrow C_2H_5OH_2^+ + C_2H_5O^-$$

The ionisation constant is $pK = 18.8$ [37] corresponding to an electrolyte concentration of the order of $\rho_{el} = 10^{-9}$ M. The Bjerrum length of ethanol is $r_b = 2.3$ nm at

room temperature and the Debye length of the solvent following from ρ_{el} is therefore of the order of $\kappa_0^{-1} = 5$ μm. This very large screening length is an upper limit, since any ionic contaminants or counter-ions will reduce the screening.

4.2. Measurements of sedimentation rates

Clear confirmation of the long-range repulsion in the sedimenting dispersions is offered by the sedimentation rates in Fig. 6. We find for all dispersions of A, B and C spheres a non-linear concentration dependence; a log–log fit of the data yields a scaling of $U \sim \varphi^{\beta}$, with $\beta \approx 0.4$. Such a non-analytical dependence and the ensuing strong concentration effects at low ϕ are typical for charged colloids with a significant contribution of counter-ions to the screening length. In the limit of no external salt the sedimentation rate follows a $\phi^{1/3}$ dependence, which changes to a linear dependence if sufficient salt is added. (This topic is extensively discussed elsewhere [21].) For the C-spheres, incidentally, a non-analytical dependence of the intrinsic viscosity at low ionic strength was recently found [25].

4.3. Visual observations of concentration profiles

In none of the samples stored as described in Section 3 did we observe during the sedimentation process any sign of floc formation or rapid settling due to aggregation. In addition, we never observed gels or any layers with a high yield stress. Interfaces and phases easily deformed under gravity, as illustrated by Figs. 2 and 13. Visual inspection showed that through the whole sedimentation process, settling silica spheres left behind a supernatant phase, which contained particles giving rise to visible (laser) light scattering, as illustrated in Figs. 7 and 8. The height of supernatant columns was as large as 20 cm (Fig. 12), corresponding to approximately 1250 gravitational lengths for the C-spheres. We could not distinguish a height dependence of the supernatant turbidity (see for example Fig. 8), which points to a fairly homogeneous particle distribution. These supernatants were found for all sedimentation vessels and all silica species in Table 1. Moreover, the very presence of such a supernatant did not seem to be affected by the temperature control: it was observed in suspensions left undisturbed in a cupboard (Fig. 2) without any precaution, in suspensions stored in a thermostatted room (Fig. 1), and in fluids thermally shielded by an additional, large water bath (Figs. 7 and 8). We note that in dispersions of uncharged silica spheres (coated with polyisobutene) in toluene, we could not visibly discern any scattering from a supernatant, neither in stock samples nor in thermally isolated vessels.

Turning back to the charged spheres, at sufficiently high starting concentration, particle deposition on the bottom of the vessel took place as indicated by a boundary, for instance as A in Fig. 1. On a time scale of weeks–months, colloidal crystal growth could be observed in nearly all of those deposits (see Fig. 11).

A striking observation was that at low initial overall density, sometimes no sedimentation took place at all; the suspension remained spatially homogeneous. This in spite of the fact that at higher starting density values, particles from exactly

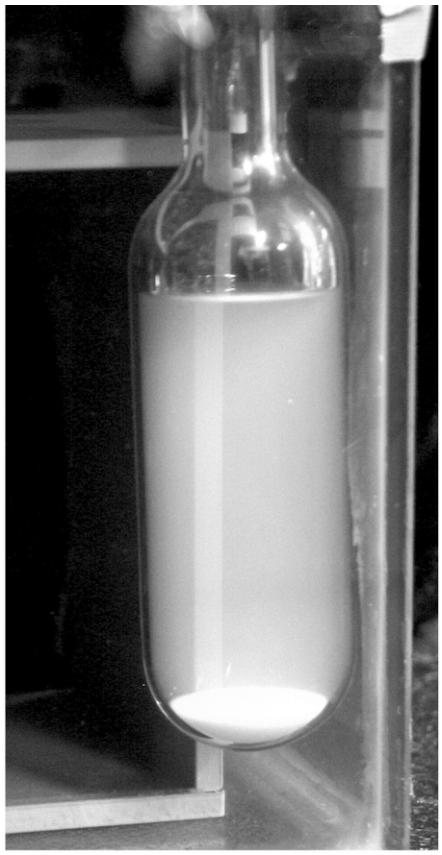

Fig. 8. C-silica dispersion in absolute ethanol, stored for 5 months in a large thermostatted aquarium in the dark, illustrating the homogeneous particle distribution in a supernatant above a still amorphous sediment.

the same silica stock did settle into a dense deposit (Fig. 11). These homogeneous suspensions and the supernatants mentioned above could persist for weeks–months, although sometimes they slowly contracted under gravity, as illustrated in Fig. 11. Also, in the tubes in Fig. 6 we noted that some supernatants started to settle after approximately at least 1 month, although the settling interface was difficult to see and easily faded away under illumination (see below).

A final significant observation is that in the sedimenting dense phase, two layers occasionally formed, separated by a sharp interface. This phenomenon occurred in samples with (Figs. 11 and 12) as well as without (Fig. 1, boundary B) thermal shielding by a water bath. It is easily overlooked, as can be verified in Fig. 11a.

4.4. Factors affecting profiles

Before drawing conclusions from the observations, we should address experimental factors that may influence (or even completely disturb) a sedimentation diffusion

(SD) profile. The SD profile, of course, may be affected by size fractionation, and it could be imagined that the dilute tail of the profile is due to the small particles of the distribution. However, AFM images [33] and TEM micrographs (Fig. 5) confirm that the spheres are fairly monodisperse and that no small 'secondary' particles are present. Furthermore, we already noted that the dispersions do not contain free (oligomeric of polymeric) TPM species, which could influence particle interactions, and hence SD profiles. With AFM we also verified that the dilute tail (the 'supernatants') of concentration profiles did not contain polymeric or other contaminants; all we could image were 'clean' silica spheres, as shown in [33]. In this respect it is also important to note the absence of resin in our dispersions. It is often overlooked that such resin may easily produce unwanted contaminants. We observed, for example, on several occasions that absolute ethanol after treatment with a mixed-bed resin [AG 501–X(8)D, Bio-Rad] exhibited significant light-scattering due to dust particles or polymeric species leaking from the resin. Size fractionation or contaminants are clearly not the cause of the inflated profiles. However, the conclusion that no fractionation at all occurs requires accurate data for particle size as a function of altitude, which are not available yet.

Insufficient thermal isolation is probably the greatest threat to an undisturbed SD profile. Even minute temperature gradients may induce convective rolls. Illuminating a sample with a modest light beam for several minutes is often sufficient to disturb a suspension–supernatant interface, as we frequently observed. We also noted that very dilute suspensions are especially susceptible to such disturbance. In a concentrated dispersion, hydrodynamic disturbances are strongly damped because of viscous dissipation in the narrow liquid regions between spheres, whereas in very dilute suspensions there is much less damping, because the isolated spheres are convected along with the solvent. Thus, one possible scenario explaining the presence of colloids in the supernatant is due to convections, which keep on stirring a dilute phase without affecting the concentrated sediment. This is one reason why we repeated the settling experiments with vessels completely immersed in a large aquarium. (The other reason was to use larger vessels to be able to analyse the supernatants afterwards.) In addition, some vessels were also placed in a closed thermostat and left undisturbed in the darkened thermostatted room. The observations for these vessels (Fig. 11) clearly confirm that profiles such as in Fig. 1 and Fig. 6a can be reproduced under conditions of rigorous thermal shielding.

4.5. Supernatants

The colloid weight concentration in the dilute upper phases ('supernatants') was determined by pipetting a volume of supernatant from vessels as in Fig. 7, a method that does not allow measurement of concentrations at various heights. Judging from the turbidity, however, the supernatants seem to be fairly homogeneous in concentration (Fig. 8). Thus, the supernatant concentrations in Table 2 can at least be seen as a representative order of magnitude. Clearly the overall concentration profiles comprise a fairly steep concentration drop going from the sediment to the dilute upper phase. Such a two-step profile is inconsistent with the Monte Carlo profiles of Biben et al. [15,16] obtained for sedimentation of charged spheres with a screened

Coulomb potential. These latter profiles have a very characteristic feature: they are practically linear at all heights, without any significant steps. Moreover, the Monte Carlo profiles for charged spheres extend further in space than for uncharged spheres, as expected, but the difference with respect to hard spheres is certainly much smaller than in our experiments. The screening length κ^{-1} was kept constant in the simulations [15,16]. Therefore, we suggest that a gradient in Debye length (Fig. 4) contributes to the experimental profiles. This contribution is at this stage difficult to quantify, since we have only an approximate second-virial correction in Eq. (20), whereas the supernatant fluid is filled with extensive double layers (see below) which certainly entail higher order terms.

We also note here the possibility that the SD profile generates an electric field, which results in an upward force on the colloids opposite to gravity. Biben and Hansen [16] indeed found in their calculations a nearly constant electric field inside a profile, which reduces the effective colloid mass. It is not clear yet whether such a 'condenser' is present in our systems and how much it would contribute to the inflation of profiles.

4.6. Light scattering of supernatants

Static light-scattering plots (Fig. 9a) from supernatants confirm the presence of monodisperse spheres, which obey the Guinier approximation:

$$I(K) \sim \exp\left[-\frac{K^2R^2}{5}\right] S(K) \tag{22}$$

where the intensity $I(K)$ is proportional to the static structure factor $S(K)$ and the exponential particle form factor containing the sphere radius R. Substituting the radius from scattering data at higher wave vector K [where $S(K)=1$] we obtain from the data in Fig. 9a the structure factors in Fig. 9b. A small but significant effect can be observed: $S(K)$ decreases at small K, manifesting long-range repulsive interactions. In view of the magnitude of K (see Fig. 7B) the spheres (with radius 63 nm) interact over distances in the micrometer range. Thus, the supernatants contain spheres surrounded by extensive double layers, which fill a considerable part of the supernatant space, resisting compression by gravity. In the dense deposit that eventually forms on the bottom of a sedimentation vessel, the screening length is relatively small due to the high counter-ion density, so spheres may approach each other closely. (Note in this respect the very close approach of spheres in the ethanol films imaged by cryo-TEM, Fig. 5.)

If a deposit prepared by centrifugation is brought in contact with empty, absolute ethanol, as in Fig. 10A, spheres escape by thermal fluctuations into the ethanol, where their diffuse double layer expands considerably. This expansion implies an entropy gain for the counter-ions at the cost of a lower ion–colloid attractive energy. We can imagine this 'evaporation' to continue until both effects compensate each other, leading to a gas–liquid equilibrium, with the supernatant concentration as a sort of osmotic vapour pressure. However, it is questionable whether a real phase

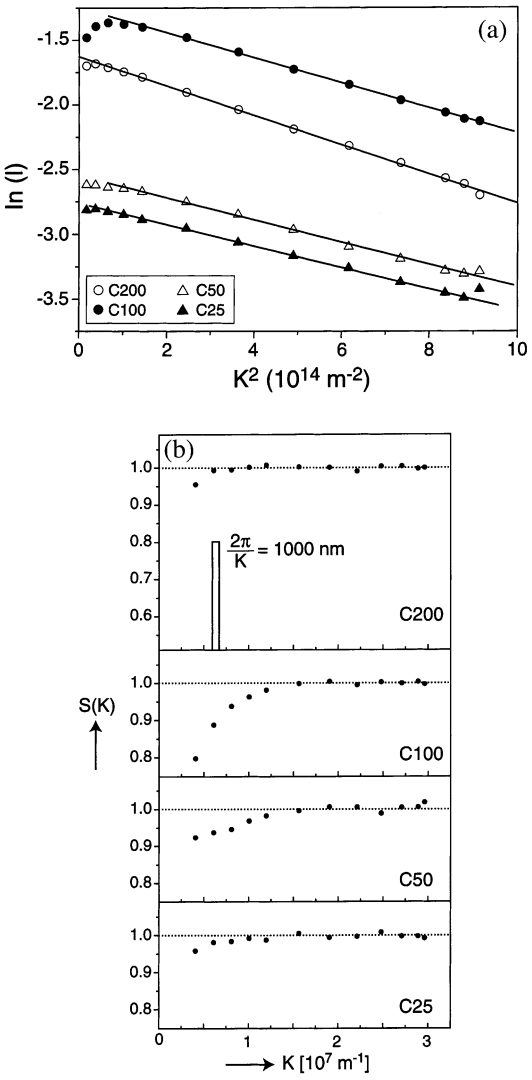

Fig. 9. (a) Logarithm of static light scattering intensities (in arbitrary units) vs. wave vector K squared, for supernatants from vessels as in Fig. 7. (b) A small but significant effect of the static structure factor $S(K)$ is present in the Guinier plots of (a), which manifest long-range repulsion. The vertical bar marks the wave vector at which $2\pi/K = 1000$ nm.

co-existence occurs in this case, and in samples such as in Figs. 7 and 8. Structure factors do not show any sign of approaching liquid–gas demixing. For example, sample C200 in Fig. 9b could be interpreted as critical, because upon increasing the concentration a sediment starts to form (see Table 2). However, the structure factor of C200 is nearly flat, which should not be the case for a critical fluid. There is no

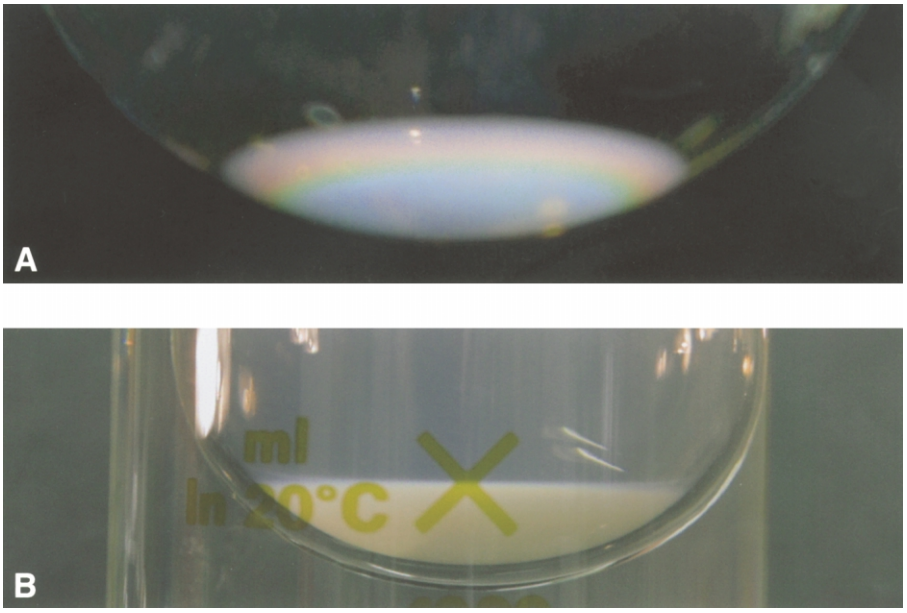

Fig. 10. (A) Typical example of a sediment of D-spheres directly after centrifugation. The coloured Bragg rings are due to the static structure factor. (B) Sample from (A) after 3-month storage of the bottle under thermostatted water in the dark. The sediment has expanded (Bragg rings have disappeared) and is partly 'evaporated', as shown by the turbidity of the supernatant.

reason yet to go beyond the hypothesis that the dilute supernatants are just an unusually long tail of a SD profile.

4.7. Denser phases

So far we have mainly discussed the dilute supernatants left behind by the majority of sedimenting silica spheres. We refer for convenience to this majority as the 'denser phase', without necessarily implying a thermodynamic equilibrium phase. Some findings for these denser phases are worthwhile documenting. We occasionally observed a fairly sharp interface separating two regions of different density, such as boundary B in Fig. 1 and p in Fig. 2. The dispersion of TPM–silica spheres in Fig. 2, previously used for a study on structure factors [36], was stored for 13 years in a cupboard. We could verify that the location of the sharp interface p did not change in at least the last 2 years. This indicates that p separates two co-existing phases. Note that the lower dense layer in Fig. 2 exhibits Bragg colours, and thus is more ordered than the amorphous upper layer, which is reminiscent of a crystal-fluid equilibrium.

We verified with another dispersion the reproducibility of such a co-existence. Fig. 13 shows a dispersion of C-spheres in an ethanol–toluene (30:70 v/v) mixture with a refractive index close to that of silica [26,36], which gives a clearer view of

the layers. The dispersion was stored for 10 years, and shows a beautiful co-existence of a region containing some crystallites with a more dilute upper layer without any crystallites. The green and blue colours are due to structure factors, as well as the optical matching [26]. The very dilute region r, incidentally, contained C-spheres of the expected size (Table 1) as verified by DLS on a drop mixed with ethanol to increase optical contrast. The sample from Fig. 13 was shaken up and divided into two tubes. After approximately 4 months, in both tubes the layering in Fig. 13 was reproduced. From drying pipetted samples, we obtained a silica weight fraction of 0.48 ($\pm$0.01) in the bottom layer, 0.32 ($\pm$0.04) in the layer between p and q, and approximately 10^{-3} in the supernatant above q. The density ratio of 1.5 seems quite large for an order–disorder transition for charged particles at low ionic strength [38]. For hard spheres the ratio is only 1.10 [39] and it is known that long-range repulsion narrows this ratio: Monte Carlo simulations show that the density ratio for solid–fluid co-existence decreases if the exponent for various inverse-power potentials increases (e.g. [39]). Hachisu et al. [40] have also shown experimentally that for charged latex spheres, the ratio of co-existing density values decreases with decreasing ionic strength. It is therefore conceivable that the density ratio for the co-existence in Fig. 13 is increased by additional (many-body) attractions. We should note, however, that a density-dependent thermodynamic excluded volume [cf. Eqs. (15) and (16)] probably also increases the relative number density difference in the order–disorder co-existence, because in the dilute phase the excluded volume per particle is greater than in the concentrated phase. A clear conclusion about the role of attractions at least requires a systematic mapping of phase diagrams of dispersions, as in Fig. 13.

The interface B in Fig. 1 is certainly not a crystal–fluid interface, and separates two disordered fluid phases. A similar interface between two amorphous regions can be observed in Figs. 11 and 12. In Fig. 12 the starting silica volume fraction was 1.4×10^{-3}, which is much too low for crystal nucleation, requiring the much higher densities in silica deposits at the bottom in Fig. 11.

5. Conclusions

The observations reported here on monodisperse silica spheres in ethanol reveal at least two important features. First, for all silica species in this study (Table 1), concentration profiles are formed with a very slowly decaying tail ('supernatant') containing low densities of spheres repelling each other over distance of micrometers. The spatial extension of the tails is not caused by thermal convections, vibrations or size fractionation, and is not observed for uncharged spheres. In addition, in view of their persistence over time, the strongly inflated profiles are very likely an equilibrium feature of the silica spheres in ethanol. They can be qualitatively explained as a consequence of entropic lift due to counter-ions, together with a density-dependent excluded volume, the latter producing an algebraic long-distance tail of the sedimentation–diffusion profile in a salt-free solvent. A rigorous equation of state for dilute colloids at very low ionic strength is needed to quantify further this explanation. An electric field may also contribute, as it decreases the effective

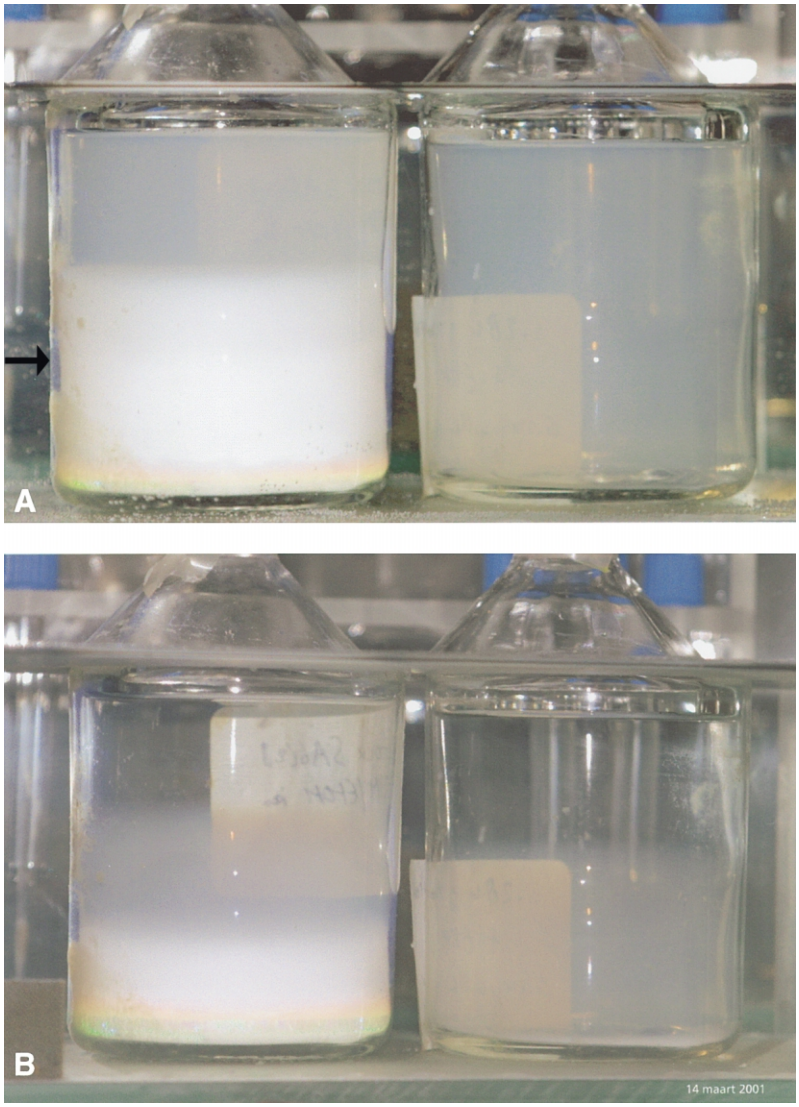

Fig. 11. (A) C-silica spheres in absolute ethanol, in bottles immersed in thermostatted water, left in the dark for 2 months. Left: the denser sedimenting phase has demixed into two layers (arrow indicates boundary). Note the presence of a Bragg reflecting colloidal crystal at the bottom. Right: no sedimentation has occurred yet. Initial concentrations are 3 g/l (*left*) and 0.6 g/l (*right*). (B) Vessels shown in (A), 2 months later. The dilute phases in both vessels have partly settled.

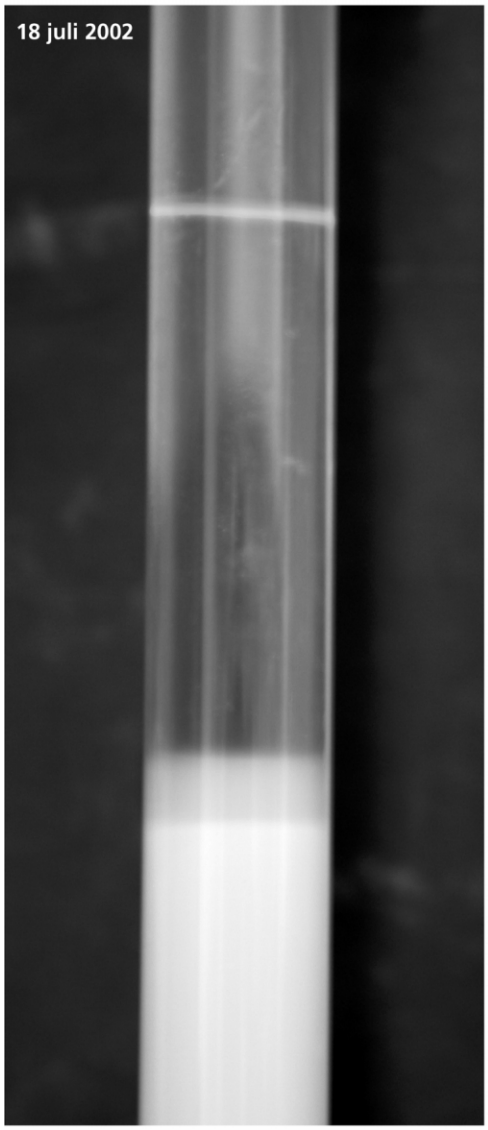

Fig. 12. Example of a C-silica dispersion (initial concentration 2.3 g/l) with a demixing sedimenting phase. The supernatant (with a red laser beam) is approximately 20 cm high. The thermally isolated dispersion was stored in the dark for 4 months. The interface in the sedimenting region fades away after exposure to light in absence of thermal shielding.

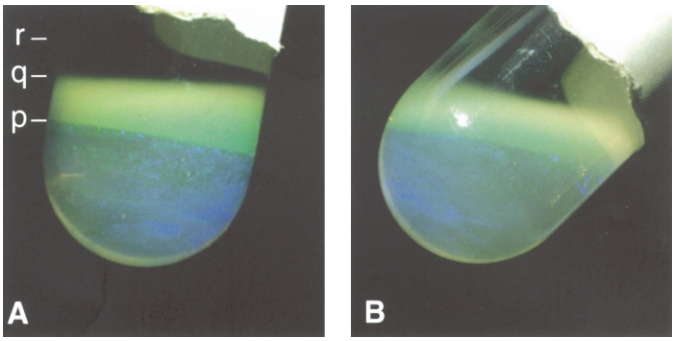

Fig. 13. C-silica spheres in an optically matching ethanol–toluene mixture [26,36]. The layering, which is about 10 years old, is a reproducible phase co-existence, as explained in the text.

mass of the spheres. There is no evidence at present that the dilute supernatants are a thermodynamic gas phase, even though the visual appearance of some dispersions (e.g. in Figs. 7 and 8) reminds of liquid–gas co-existence.

The second important feature of the silica dispersions observed is that the denser phase, which settles out of the dilute supernatant, often demixes into two (disordered) layers of different density. Quantitative information about these layers is lacking and their formation kinetics is still unclear. However, the phenomenon clearly exists, and seems difficult to explain without assuming the presence of many-body attractions; there is no doubt that the particles are repulsive on the pair level. Dispersions that have completely equilibrated under gravity (Figs. 2 and 13) exhibit a two-phase coexistence, with a density ratio that is significantly greater than expected for an order–disorder transition, although a firm conclusion about the role of (many-body) attractions requires a quantitative experimental phase diagram and a better theoretical understanding of the effect of a density-dependent excluded volume. The supernatant above the two-phase equilibrium is, again, a very dilute dispersion (Figs. 2 and 13), which we now can identify as the long-distance tail of the SD profile of the upper phase.

Acknowledgments

We would like to acknowledge the stimulating discussions with Dr R. van Roij and Dr M. Dijkstra on the topic of charged colloids. Photographs and figures were prepared by J. den Boesterd and I. van Rooijen. K. Rietveld, I. Dur and P. de Graaf are thanked for the skilful construction of glassware and sedimentation equipment. Dr P. Frederik and Mr P. Bomans (Maastricht University) generated the cryo-TEM images and Dr M. Rasa the AFM images; N. Zuiverloon synthesised the D-spheres, and S. Sacanna and M. Pazzini prepared the A and B spheres. Dr S. Williams contributed to Appendix A and Profs H. Lekkerkerker and A. Vrij are acknowledged for useful comments. Marina Uit de Bulten and Mieke Lanen assisted skilfully with the preparation of the final manuscript.

Appendix A: Second virial coefficient

The double-layer repulsion in the DLVO potential for two spheres of diameter σ at a centre-to-centre distance r for the case of a weak double-layer (DL) overlap is [1]:

$$\frac{V^{\mathrm{DL}}(r)}{kT} = C\frac{\sigma}{r}\exp\left[-\kappa(r-\sigma)\right] \tag{A1}$$

The contact value of this screened Coulomb potential at $r=\sigma$ is:

$$C = \frac{\pi\varepsilon\varepsilon_0\sigma}{kT}\psi_0^2 = \frac{1}{4}\frac{\sigma}{r_{\mathrm{b}}}y_0^2 \tag{A2}$$

in which $y_0 = e\psi_0/kT$ is the reduced surface potential on the sphere surface. The second virial coefficient is:

$$B_2 = 2\pi\int_0^{\infty}\left(1-\exp\left[-\frac{V(r)}{kT}\right]\right)r^2\mathrm{d}r \tag{A3}$$

The potential is that of a hard-sphere at $r<\sigma$, so $V(r)$ in Eq. (A3) equals:

$$\begin{aligned} V(r) &= \infty \qquad \text{for} \quad 0 \le r < \sigma \\ &= V^{\mathrm{DL}}(r) \qquad \text{for} \quad r \ge \sigma \end{aligned} \tag{A4}$$

For an uncharged hard sphere (denoted by HS) $V^{\mathrm{DL}}(r)$ equals zero. Thus, $B_2^{\mathrm{HS}} = (2/3)\pi\sigma^3$ and Eq. (A3) can be rewritten in the dimensionless form:

$$\frac{B_2}{B_2^{\mathrm{HS}}} = 1+3\int_1^{\infty}\left(1-\exp\left[-V(x)\right]\right)x^2\mathrm{d}x \tag{A5}$$

$$V(x) = \frac{C}{x}\exp\left[-\kappa\sigma(x-1)\right]; \qquad x = \frac{r}{\sigma} \tag{A6}$$

For weak double-layer potentials the exponent in Eq. (A5) can be linearised to yield:

$$\frac{B_2}{B_2^{\mathrm{HS}}} = 1+3C\frac{(1+\kappa\sigma)}{(\kappa\sigma)^2} \tag{A7}$$

For higher potentials B_2 can be approximated using an effective hard-sphere with a weak perturbation. The effective diameter d_i is the centre-to-centre distance at which the repulsion between two spheres equals kT (a sort of Bjerrum length for colloidal spheres):

$$C\frac{\sigma}{d_i}\exp\left[-\kappa(d_i-\sigma)\right] = 1 \tag{A8}$$

We assume, therefore, the following potential:

$$V(r) = \infty \qquad \text{for} \quad 0 \le r < d_i$$
$$= V^{\mathrm{DL}}(r) \ll kT \qquad \text{for} \quad r \ge d_i \tag{A9}$$

which yields:

$$B_2 = \frac{2}{3}\pi d_i^3 \left[1 + \frac{3(1+\kappa d_i)}{(\kappa d_i)^2} \right] \tag{A10}$$

Next we approximate the colloidal Bjerrum length via:

$$d_i = \sigma + a\kappa^{-1}; \quad a \ge 0 \tag{A11}$$

and assume that for large enough κ^{-1} only the leading term in Eq. (A10) is important. This gives the scaling:

$$\left(\frac{B_2}{B_2^{\mathrm{HB}}} \right)^{1/3} \approx \kappa \frac{\kappa^{-1}}{\sigma} \quad \text{for} \quad \frac{\alpha\kappa^{-1}}{\sigma} \gg 1 \tag{A12}$$

Comparison with numerical integrations of Eq. (A5) shows that Eq. (A12) gives a reasonable estimate for the numerical B_2 for $\kappa\sigma < 2$ and a wide range of C, with α-values in the range $\alpha = 3$–4.

References

[1] E.J.W. Verwey, J.Th.G. Overbeek, Theory of the Stability of Lyophobic Colloids, Dover, Mineola, 1999.
[2] B. Beresford-Smith, D.Y.C. Chan, D.J. Mitchell, J. Colloid Interface Sci. 105 (1985) 216.
[3] A. Klinkenberg, J.L. van der Minne, Electrostatics in the Petroleum Industry, Elsevier, Amsterdam, 1958.
[4] B.V.R. Tata, E. Yamahara, P.V. Rajamani, N. Ise, Phys. Rev. Lett. 78 (1997) 2660.
[5] E. Ruckenstein, Adv. Colloid Interface Sci. 75 (1998) 169.
[6] R. van Roij, J.-P. Hansen, Phys. Rev. Lett. 79 (1997) 3082.
[7] R. van Roij, J.-P. Hansen, Progr. Colloid Polym. Sci. 110 (1998) 50.
[8] R. van Roij, M. Dijkstra, J.-P. Hansen, Phys. Rev. E 59 (1999) 2010.
[9] R. van Roij, R. Evans, J. Phys.: Condens. Matter 11 (1999) 10047.
[10] P. Linse, V. Lobaskin, Phys. Rev. Lett. 83 (1999) 4208.
[11] D. Chan, P. Linse, S.N. Petris, Langmuir 17 (2001) 4202.
[12] M.E. Fisher, Y. Levin, Phys. Rev. Lett. 71 (1993) 3826.
[13] J.M. Romero-Enrique, G. Orkoulas, A.Z. Panagiotopoulos, M.E. Fisher, Phys. Rev. Lett. 85 (2000) 4558.
[14] V. Degiorgio, R. Piazza, T. Bellini, in: M. Baus, et al. (Eds.), Observation, Prediction and Simulation of Phase Transitions in Complex Fluids, Kluwer Academic Press, 1995.
[15] T. Biben, J.P. Hansen, J.L. Barrat, J. Chem. Phys. 98 (1993) 7330.
[16] T. Biben, J.P. Hansen, J. Phys: Condens. Matter A 6 (1994) 345.
[17] A.P. Philipse, Curr. Opin. Colloid Interface Sci. 2 (1997) 200.
[18] D.M.E. Thies-Weesie, A.P. Philipse, Langmuir 11 (1995) 4180.
[19] D.B. Siano, J. Colloid Interface Sci. 68 (1978) 111.
[20] W. van Saarloos, D.A. Huse, Europhys. Lett. 11 (1990) 106.

[21] D.M.E. Thies-Weesie, A.P. Philipse, G. Nagele, B. Mandl, R. Klein, J. Colloid Interface Sci 176 (1995) 43.
[22] K.J. Mysels, Introduction to Colloid Chemistry, Wiley, New York, 1967.
[23] A. Vrij, J. Chem. Phys. 72 (1980) 3735.
[24] J.K.G. Dhont, An Introduction to Dynamics of Colloids, Elsevier, Amsterdam, 1996.
[25] Y. Dziechciarek, J.J.G. van Soest, A.P. Philipse, J. Colloid Interface Sci. 246 (2002) 48.
[26] A.P. Philipse, A. Vrij, J. Colloid Interface Sci. 128 (1989) 121.
[27] G.H. Koenderink, A.P. Philipse, J. Chem. Phys., in press.
[28] P.M. Frederik, W.M. Busing, J. Microsc. 144 (1986) 215–221.
[29] P.M. Frederik, M.C.A. Stuart, A.H.G.J. Schrijvers, P.H.H. Bomans, Scanning Microsc. 3 (Suppl.) (1989) 277–284.
[30] Y. Talmon, Ber. Bunsenges. Phys. Chem. 100 (1996) 364–372.
[31] L.N. Donselaar, P.M. Frederik, P.H. Bomans, P.A. Burning, B.M. Humbel, A.P. Philipse, J. Magn. Magn. Matter 201 (1999) 58–61.
[32] P.M. Frederik, P.H.H. Bomans, P.F.J. Laeven, F.J.T Nijpels, Device for Preparing Specimens for a Cryo-Electron Microscope, Netherlands Industrial Property Office (RO/NL), 2002, PCT/NL02/00189.
[33] M. Rasa, B.W.M. Kuipers, A.P. Philipse, J. Colloid Interface Sci. 250 (2002) 303.
[34] J.S. van Duijneveldt, J.K.G. Dhont, H.N.W. Lekkerkerker, J. Chem. Phys. 99 (1993) 6941.
[35] A.P. Philipse, B.C. Bonekamp, H.J. Veringa, J. Am. Ceram. Soc. 73 (1990) 2720.
[36] A.P. Philipse, A. Vrij, J. Chem. Phys. 88 (1988) 6459.
[37] J.R. Chipperfield, Non-Aqueous Solvents, Oxford, University Press, 1998.
[38] R. van Roij, personal communication.
[39] E.L. Pollock, J.P. Hansen, Phys. Rev. A 8 (1973) 3110.
[40] S. Hachisu, Y. Kobayashi, A. Kose, J. Colloid Interface Sci. 42 (1973) 342.